FERMILAB-CONF-77-121-E

E214

CALT 68-567
ENERGY RESEARCH AND
DEVELOPMENT REPORT

DIMUON AND TRIMUON PRODUCTION IN HIGH ENERGY NEUTRINO AND ANTINEUTRINO INTERACTIONS*

B. C. Barish, J. F. Bartlett, A. Bodek, K. W. Brown, D. Buchholz†,
Y. K. Chu, F. Sciulli, E. Siskind. L. Stutte††,
California Institute of Technology, Pasadena, California 91125
E. Fisk, G. Krafczyk, D. Nease
Fermilab, Batavia, Illinois 60510
and
O. Fackler
Rockefeller University, New York, N.Y. 10021

Talk presented by O. Fackler at the Division of Particles and Fields Meeting, Brookhaven National Laboratory, Upton, New York, October 6-8, 1976.

* Work supported in part by the U.S. Energy Research and Development Administration. Prepared under Contract E(11-1)-68 for the San Francisco Operations Office.

† Now at Northwestern University, Evanston, Illinois 60201.

†† Now at Fermilab, Batavia, Illinois 60510

I. Introduction

We are reporting on studies of dimuon production in the high energy neutrino and antineutrino induced events accrued during an experiment to measure normalized neutrino and antineutrino cross sections. This report describes the results of a more detailed analysis of the data discussed in ref. 1. These data were obtained in the fall of 1975 using the Caltech-Fermilab apparatus,[2] the narrow band dichromatic neutrino beam,[3] and were taken over a wide range of separate incident neutrino energies, between 30 and 220 GeV, corresponding to hadron beam energy settings of 80-250 GeV. The spill time was long enough (~1 sec) to allow for independent determination of the incident neutrino flux. The total data sample for which most kinematic quantities are calculable consists of approximately 18,000 single muon charged current events.

Some features of the experiment that are particularly relevant to dimuon or trimuon studies are:

1) the sign selected beam - This beam allows for clear separation and study of events induced by neutrinos or antineutrinos. The measured wideband antineutrino event background is approximately 2% in the neutrino data. The corresponding neutrino wideband event background is measured to be about 5% in the antineutrino data.

2) a variable ν ($\bar{\nu}$) beam energy - Since the mean incident energy is known to ± 5% and the uncertainty in the neutrino energy is approximately ±20%, we can investigate the energy dependence of the multimuon signal.

3) the peaked structure of the dichromatic beam - This beam allows, by the conservation of energy, determination of whether significant energy is carried away by neutrinos. Figure 1 shows the observed energy distribution for neutrino induced events obtained with the secondary hadron beam line set to transport a 250 GeV beam through

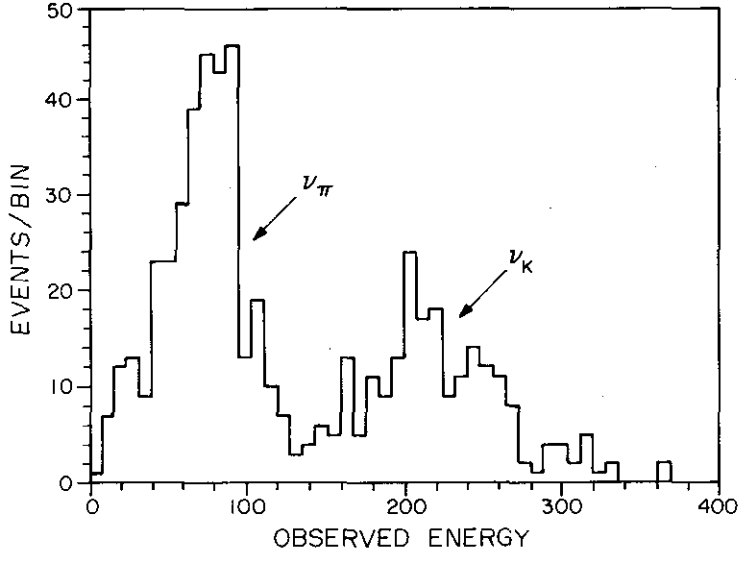

Figure 1

The observed energy distribution for neutrino induced events with the secondary hadron beam line set to transport a 250 GeV beam through the decay pipe. Two peaks in the neutrino spectrum are the result of decays of pions (ν_π) and kaons (ν_K).

the decay pipe. Two peaks in the neutrino spectrum are the result of decays of pions and kaons in the decay pipe.

4) a dense target - The packing fraction of the target-calorimeter is approximately 50% (i.e. the density is about 4 gm/cm^3), which minimizes extra muons from pion or kaon decay. However, the target, being only one density, allows no empirical check of the prompt versus the non-prompt signal.

5) good muon identification - Since the target also serves as the muon-identifier, it is well instrumented to study muons down to an energy where muons and pions cannot be distinguished ($\sim$ 2 GeV). Any "punch-thru" problem cannot be studied internally because of the continuous nature of the muon identifier.

6) a small solid angle magnet - Many identified second muons do not traverse the spectrometer because they are too low in energy or at too large an angle. This is a severe limitation in the data analysis since the more complete kinematic information is only determined for the fraction of the events traversing the magnet.

We are concentrating our studies of the data on answering the following questions:

1) Is there a signal for antineutrino induced dimuon events above background?

2) If there is an antineutrino induced signal, how do the rates and features compare with neutrinos?

3) What is the observed energy dependence of the dimuon versus single muon signal?

4) Are there trimuons produced in neutrino or antineutrino interactions and if so, what is the rate?

The results are still preliminary, mainly because the hadron energy calibration is not yet finished. Consequently, there is presently a ±20% uncertainty in the hadron energy. This uncertainty is reflected in some of the kinematic quantities and in the pion and kaon background level relative to the data.

The background calculations are also preliminary and consequently no background subtractions have been made.

The search for multimuon events has been completed, while only a partial sample of single muon charged current events has been studied at this time. Roughly 10-30% of the single muon events have been measured (depending on the energy) so that the total numbers of single muon events have been estimated.

The dimuon data presented here have only been corrected for the azimuthal detection efficiency because any further correction requires a knowledge of the dimuon production mechanism.

II. General Features of the Events

Figures 2 a,b show two dimuon events observed with the beam set to transport a positive 190 GeV/c secondary beam through the decay pipe. The neutrinos enter from the left and interact in the 140 ton steel target. Scintillation counters located every four inches of steel were used to measure the final state hadron energy E_H using calorimetry techniques.[4] The angles of the final state muons θ_μ were determined with spark chambers inside the steel target. A steel toroid downstream of the target was used to measure the momentum of muons which traversed it.

Figure 2a shows an event with rather large hadron energy in which both muons enter the spectrometer. The total energy observed ($\sim$180 GeV) is so large that this event must have come from a kaon-decay neutrino ($<E_{\nu K}> \simeq 170$ GeV). Figure 2b shows perhaps a more typical event in which both muons leave the target and the total energy is a lower limit.

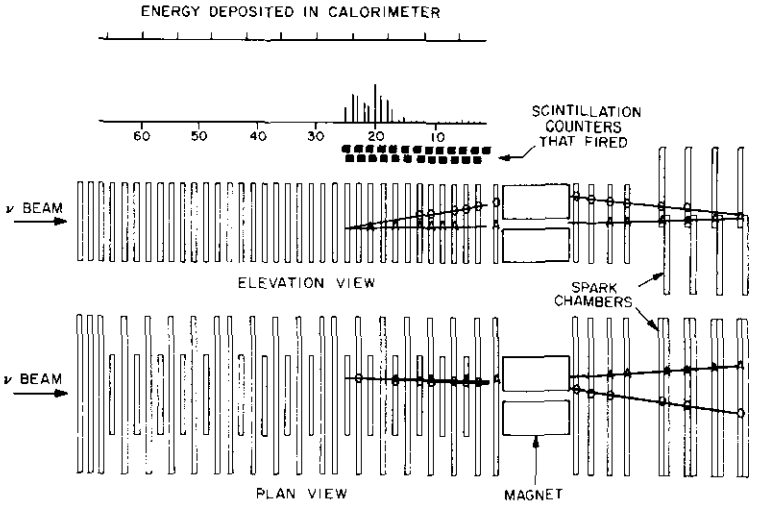

Figure 2 a

An example of a dimuon candidate observed with a +190 GeV secondary hadron beam. Both muons enter the magnetic spectrometer. The total energy observed is 180 GeV so that this event must have been induced by a kaon neutrino (ν_K).

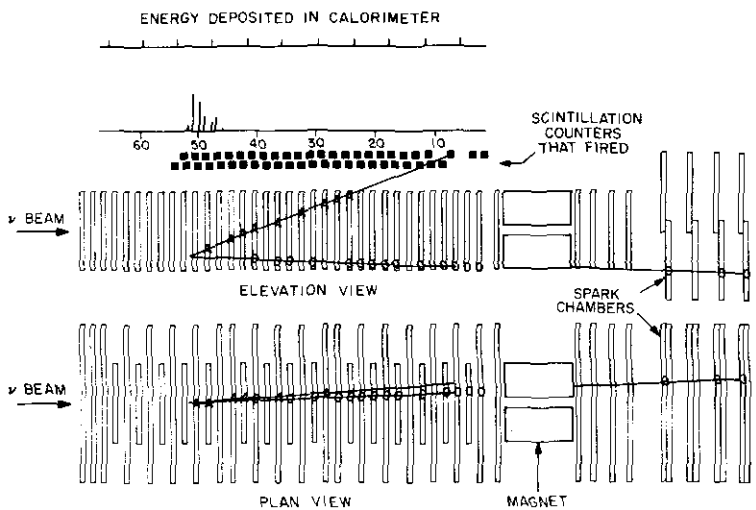

Figure 2 b

An example of a dimuon candidate observed with a +190 GeV secondary hadron beam. Both muons leave the detector before entering the spectrometer magnet.

III. Event Selection

Table 1 summarizes the number of events at the different stages in the event selection process.

	Number of ν Induced Events	Number of $\bar{\nu}$ Induced Events	Sum
Single μ events in which 1μ enters the spectrometer (estimated)	~12,000	~6,000	~18,000
2μ candidates in which 1μ enters the spectrometer	169	54	223
2μ events in which 1μ enters the spectrometer and the other traverses more than 1.8 meters of steel	90	33	123
2μ events in which 1μ enters the spectrometer and the other traverses more than 2.8 meters of steel	41	15	56
2μ events with both muons entering the spectrometer -			
Opposite Sign Muons	13	8	21
Same Sign Muons	2	0	2
3μ Events	2	0	2

Table 1

The number of observed events at various stages in the event selection process.

IV. Backgrounds

The dimuon event background arises mainly from a normal single muon event in which: 1) a hadron in the hadron shower has a particularly long penetration, or 2) a pion or kaon in the hadron shower undergoes a $\mu\nu$ decay. These backgrounds are reduced and the second muon identified by placing a penetration requirement on the second track.

The problems of muon identification can be studied by plotting the ratio of the average pulse height in two counters upstream to the average pulse height in two counters downstream of the second muon stopping point as a function of the second muon penetration, $L_{\mu 2}$. Figure 3 shows this ratio versus $L_{\mu 2}$ for the dimuon candidates. This ratio should be two for a stopping muon since there are two muons passing through the counters upstream of this point and only one downstream. It would be different from two if we were observing the tail end of the hadron shower. The data are consistent with events having a stopping muon down to a penetration of about 1.5 meters.

The most likely source of background for dimuon events is an ordinary charged current event with an extra muon resulting from the decay of a pion or kaon produced in the hadronic cascade. Unfortunately we have no direct measure of this non-prompt background because the target is uniform in density.

In order to estimate this background, we have used a Monte Carlo program to simulate the hadronic cascade through several generations until the shower is completely absorbed in the target-calorimeter. The final state hadron distributions in the initial neutrino interaction were chosen to match the multiplicity and energy distributions for charged hadron interactions in iron. The resulting probability curves are folded with the measured hadron energy (E_H) distributions at each incident neutrino energy to obtain the expected number of background two muon events originating from pion and kaon decays.

Figures 4 a,b,c,d show the integrated number of two muon events as a function of the second muon penetration, $L_{\mu 2}$, with $L_{\mu 2} > L$. In order to compare with the single muon data and to make a meaningful analysis only dimuon candidates where at least one muon entered the spectrometer are plotted. The neutrino and antineutrino data are shown separately. The data in each sample are further classified as to whether the events were produced by low energy incident neutrinos, resulting from pion decay (ν_π), or whether the events

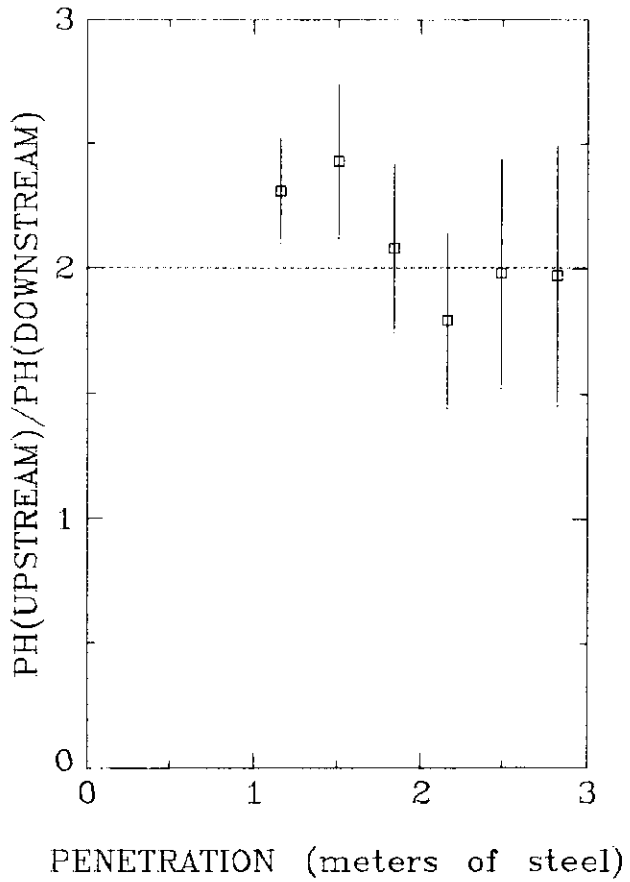

Figure 3

To study muon identification, the ratio of pulse height in two counters upstream to two counters downstream of the second muon stopping point is plotted as a function of the second muon penetration, $L_{\mu 2}$. The data are consistent with the expected ratio of two for a stopping second muon for $L_{\mu 2} \geq 1.5$ meters of steel.

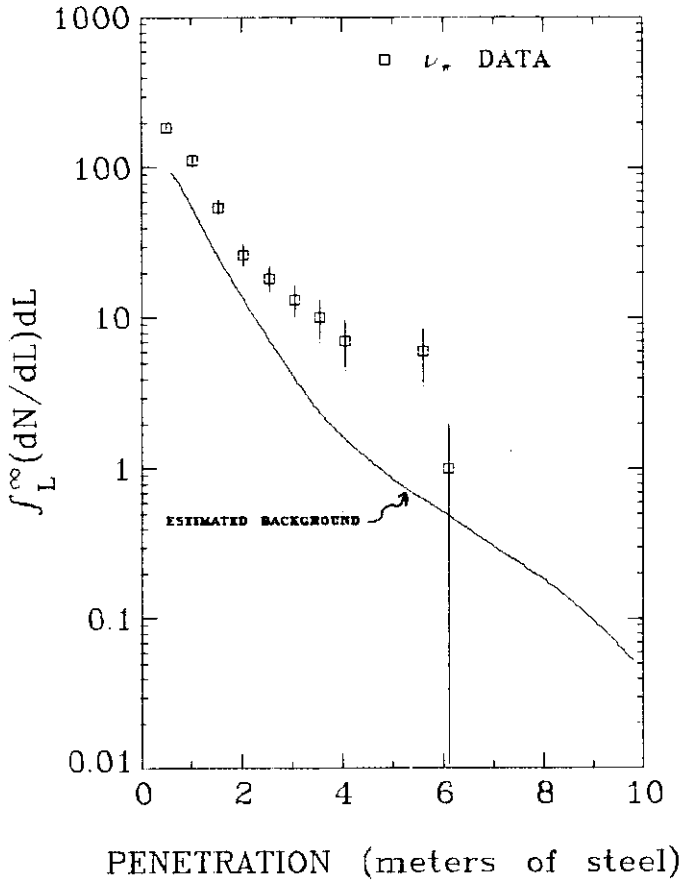

Figure 4 a

To study the non-prompt background from pion and kaon decay in the hadron shower, the integrated number of ν_π induced events is shown as a function of the second muon penetration, $L_{\mu 2}$, with $L_{\mu 2} > L$. The smooth curve is the estimated non-prompt background.

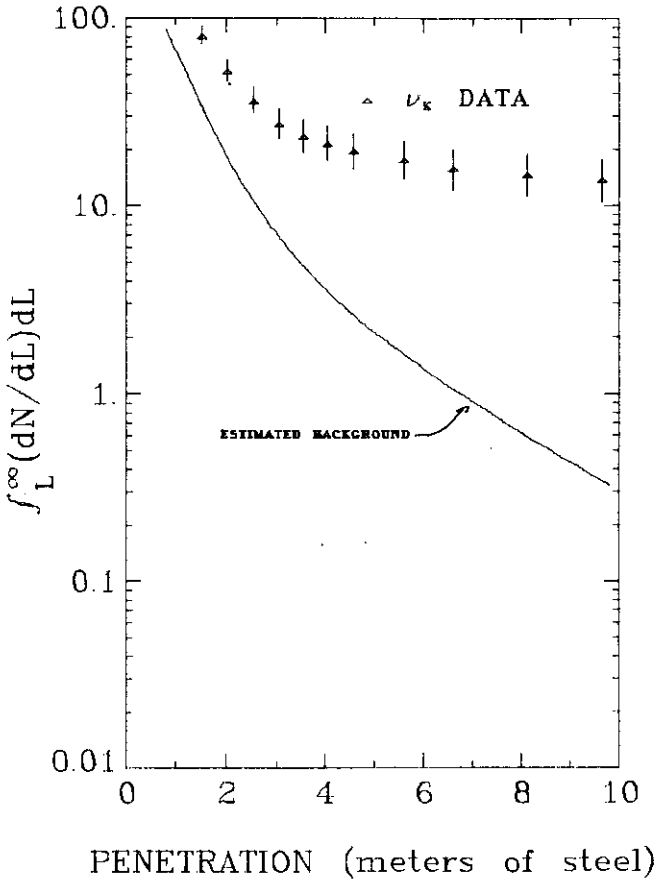

Figure 4 b

To study the non-prompt background from pion and kaon decay in the hadron shower, the integrated number of ν_K induced events is shown as a function of the second muon penetration, $L_{\mu 2}$, with $L_{\mu 2} > L$. The smooth curve is the estimated non-prompt background.

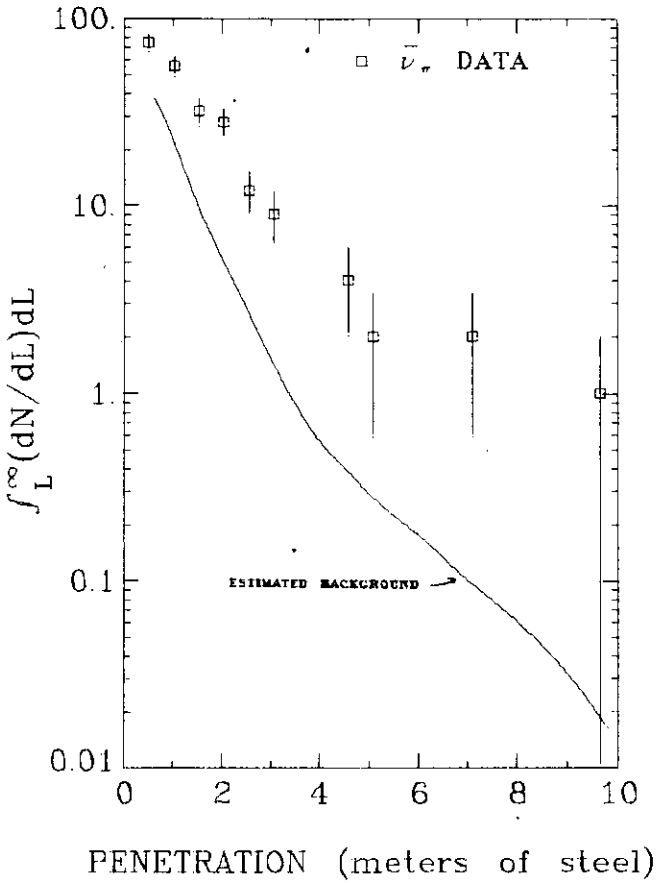

Figure 4 c

To study the non-prompt background from pion and kaon decay in the hadron shower, the integrated number of $\bar{\nu}_\pi$ induced events is shown as a function of the second muon penetration, $L_{\mu 2}$, with $L_{\mu 2} > L$. The smooth curve is the estimated non-prompt background.

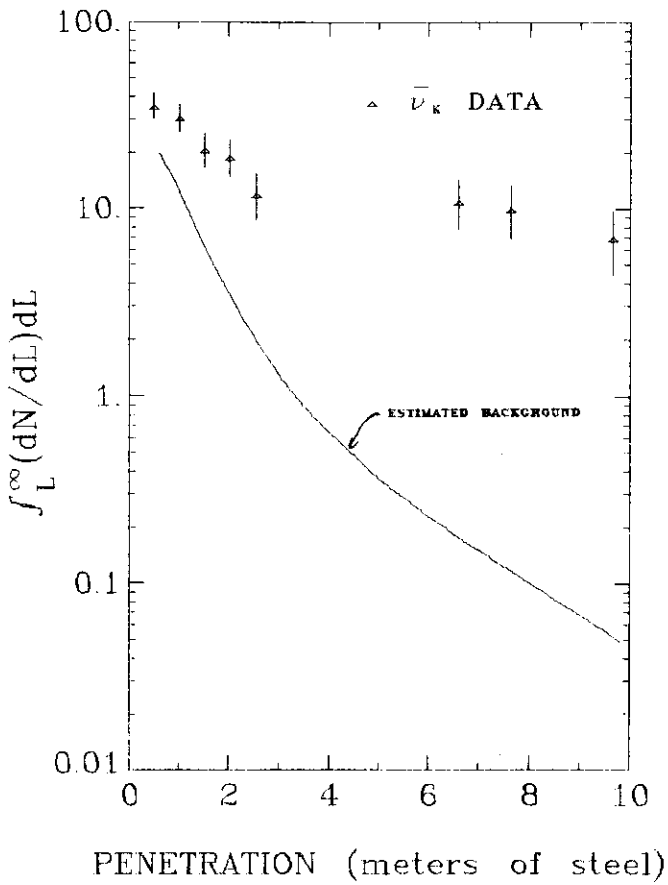

Figure 4 d

To study the non-prompt background from pion and kaon decay in the hadron shower, the integrated number of $\bar{\nu}_K$ induced events is shown as a function of the second muon penetration, $L_{\mu 2}$, with $L_{\mu 2} > L$. The smooth curve is the estimated non-prompt background.

were produced by high energy neutrinos, resulting from kaon decay (ν_K). The hadron energy distributions, and consequently their decay probabilities, are very different for these two categories. The data in each sample are summed over the incident energies. The equivalent penetration is plotted for those events in which the second muon passed through the spectrometer (a muon penetration of 10 meters of steel requires about 14 GeV). The smooth curves are the result of the Monte Carlo background calculation.

This calculation has been compared with data on muon penetration taken previously with hadrons of 50 and 100 GeV incident on a test calorimeter. The calculation agrees with the data; however, the test device is smaller in both cross section and longitudinal extent than the actual calorimeter used in this experiment. Also, the test data are somewhat limited statistically. Finally, the assumption that the hadronic final state from neutrino collisions is identical to that from hadron collisions has not been demonstrated, although certain similarities have been seen. For these reasons we feel that the background calculation is presently uncertain by approximately a factor of two for the second muon penetration less than about three meters of steel and as much as a factor of five for the second muon penetration greater than about five meters of steel. (We are presently setting up to measure the background empirically.) This means that for the data presented here, the qualitative features are likely to be preserved after the background has been subtracted.

It is apparent that any background resulting from pion and kaon decay is most serious for low energy second muons. Consequently we have also analyzed the data with a longer penetration requirement ($L_{\mu 2} > 2.8$ meters of steel) on the second muon, giving a "purer" but more biased sample than the one requiring $L_{\mu 2} > 1.8$ meters of steel. The average kinematic quantities calculated for these two samples (e.g. x, y, W^2, etc.) are statistically the same. Hence any background which might be in the sample with the requirement the $L_{\mu 2} > 1.8$ meters of steel does not affect the kinematic averages at our statistical level.

As a consequence of these studies on muon identification and background levels, for further analysis we will mainly consider the dimuon sample having at least one muon entering the spectrometer (in order to compare with the single muon charged current data) and the other penetrating more than 1.8 meters of steel.

V. Energy Dependence of Dimuon Production

The observed energy distribution for a sample of single muon events obtained at a hadron beam setting of +190 GeV is shown in figure 5. The observed energy distribution for the dimuon events is also shown (the scale of the ordinate is arbitrary). The dimuon energy distribution is consistent with the single muon energy distribution shown in the same figure. Indeed, this would be the case if an unseen final state lepton carried away only a small fraction of the total energy.

To study the energy dependence of the dimuon production rate, we have classified the dimuon events into two distinct energy bands according to their total observed energy. At a given beam energy setting, if the observed dimuon energy is greater than the energy where the valley between the ν_π and ν_K peaks is located, the event is classified as having been induced by a ν_K with an energy equal to the mean ν_K energy. Otherwise the event is classified as being

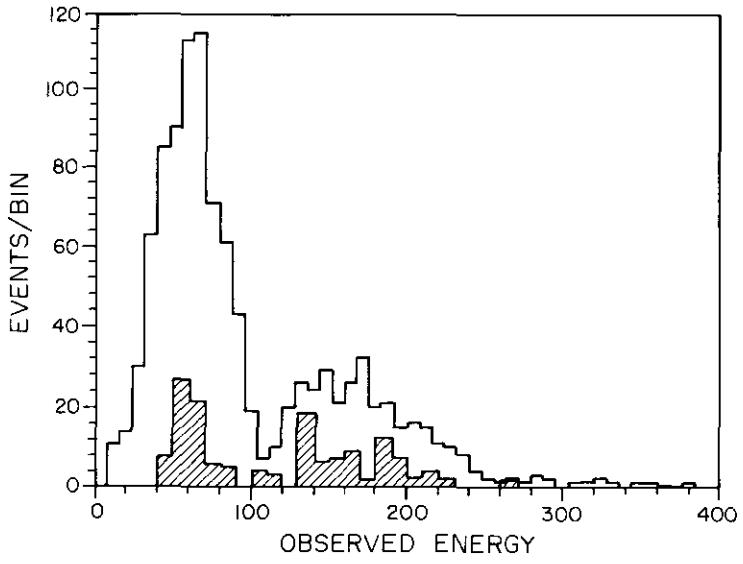

Figure 5

In order to investigate whether an unseen, final state lepton carries away a substantial amount of energy, the single muon and dimuon (cross hatched) energy distributions are shown. These two distributions are not relatively normalized. The azimuthally corrected dimuon distribution is plotted with a magnified scale and contains 148 corrected events. The dimuon energy distribution is consistent with the single muon distribution suggesting a relatively small amount of "missing energy".

induced by a ν_π with an energy equal to the mean ν_π energy.

To compare the average observed energy of dimuon events ($E_{\mu\mu}^{obs}$) with the average observed energy of single muon events (E_{μ}^{obs}), we define the "fractional missing energy", $\Delta \equiv (E_{\mu}^{obs} - E_{\mu\mu}^{obs}) / E_{\mu}^{obs}$ which is plotted in figure 6 as a function of the incident energy. This quantity would be positive for events with substantial missing energy (e.g. unmeasured muon energy or final state neutrinos). Two mechanisms exist which can make Δ negative: 1) misassignment of the neutrino energy (actually a ν_K when called a ν_π), and 2) a stronger energy dependence of the dimuon cross section. The two effects could combine to make Δ negative by as much as 10-15% and thereby "mask" a small amount of missing energy from final state neutrinos. On the average $\Delta \sim -0.06$. We conclude, therefore, that the observed events do not have missing energy greater than 15% of the incident neutrino energy.

The ratios of dimuon to single muon event rates ($\sigma_{\mu\mu}/\sigma_{\mu}$), corrected for the azimuthal detection efficiency, are shown as a function of the average incident energy for neutrino induced events in figure 7a and for antineutrino induced events in figure 7b. All events are included in the plots in which a) the first muon entered the spectrometer ($\theta_{\mu 1} \leq 100$ mrad) and b) the penetration of the second muon is greater than 1.8 meters of steel ($E_{\mu 2} > 2.4$ GeV). Applying more than an azimuthal efficiency correction would require a knowledge of the dimuon production mechanism (e.g. the fraction of the second muons with penetrations less than 1.8 meters of steel). Also shown in these figures are the previous Caltech-Fermilab results at 50 and 170 GeV[5] and the results from the Harvard-Penn-Wisconsin-Fermilab experiment.[6] The HPWF data differ from our data in that a) their first muon angular acceptance extends to $\theta_{\mu 1} \simeq 225$ mrad b) the second muon energy acceptance extends down to 4 GeV, and c) their data were obtained with a wide band neutrino spectrum, so their cross sections are integrated over a wide neutrino energy spectrum.

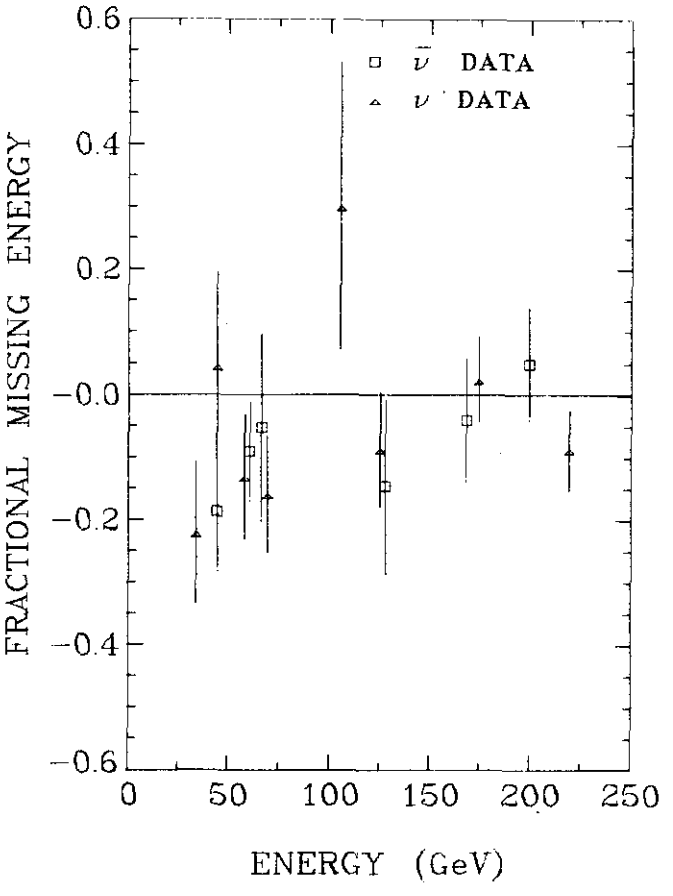

Figure 6

To compare the average observed energy of dimuon events ($E_{\mu\mu}^{obs}$) with the average observed energy of single muon events (E_{μ}^{obs}), the fractional missing energy ($=(E_{\mu}^{obs} - E_{\mu\mu}^{obs}) / E_{\mu}^{obs}$) is plotted as a function of the incident energy. This distribution is consistent with no more than 15% missing energy.

The solid curves in figures 7 a,b show our estimate of the non-prompt background from pion and kaon decay in the hadron shower. This background calculation is at most uncertain by a factor of two. Even if the calculation were a factor of two low, the background level is inconsistent with the observed $\sigma_{\mu\mu}/\sigma_{\mu}$ level and does not easily account for the increase in these ratios with energy.

Figures 8 a,b show the ratios, $\sigma_{\mu\mu}/\sigma_{\mu}$, for neutrino and antineutrino induced events as a function of the average incident energy for those events in which a) the first muon enters the spectrometer ($\theta_{\mu 1} \leq$ 100 mrad) and b) the second muon penetration is greater than 2.8 meters of steel (corresponding to $E_{\mu 2} > 4$ GeV). The solid curves show the calculated non-prompt background. The $\sigma_{\mu\mu}/\sigma_{\mu}$ ratios for this "purer" data sample are a little less but show the same qualitative energy dependence as the data with the second muon penetration greater than 1.8 meters of steel, whereas the calculated non-prompt background is considerably less. The same qualitative behavior of these two data samples is further evidence that the increase in $\sigma_{\mu\mu}/\sigma_{\mu}$ with energy is not due to an increase in the non-prompt background level.

The dashed curve drawn in figure 8a shows the calculation by Sehgal and Zerwas[7] of the expected $\sigma_{\mu\mu}/\sigma_{\mu}$ ratio based on a charm model. The curve has been normalized to the neutrino induced data at 175 GeV. The major difference between the data and the calculation is that the calculation assumes an acceptance for the first muon extending to 225 mrad whereas the first muon acceptance extends to about 100 mr for this data. The calculated energy dependence of $\sigma_{\mu\mu}/\sigma_{\mu}$ agrees reasonably well with the data. At the present time, a low mass threshold of the charm type cannot be ruled out as the sole source of dimuons.

If the second muon were associated with the hadron shower and had a relatively small angle with respect to the hadron shower direction, the second muon would approximately lie in the plane formed by the incident neutrino and

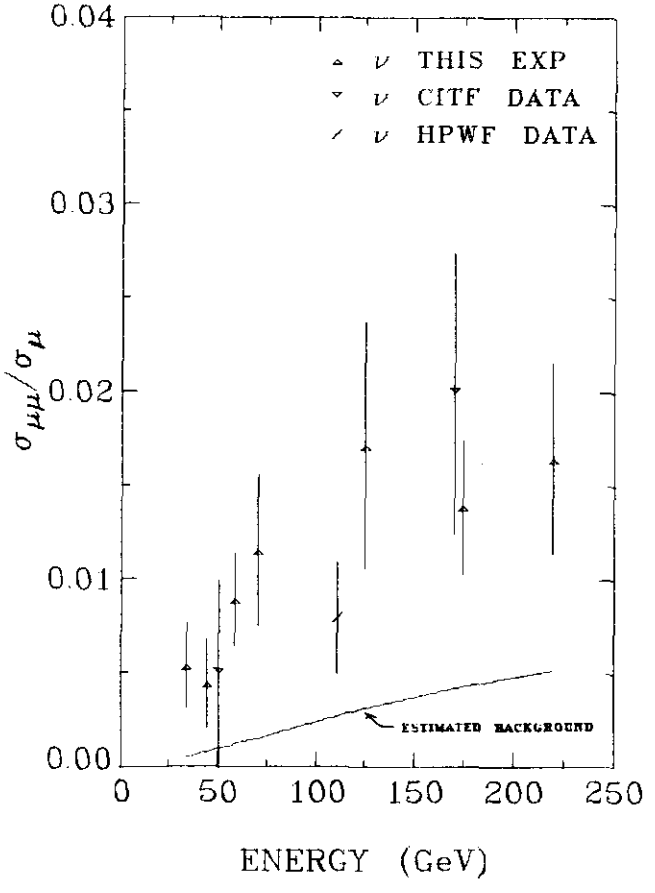

Figure 7 a

The ratio of the dimuon production cross section ($\sigma_{\mu\mu}$) to the single muon production cross section (σ_{μ}) for neutrino induced events in which the first muon enters the spectrometer and the second muon penetration is greater than 1.8 meters of steel (equivalent to 2.4 GeV) is shown as a function of incident energy. The results described in ref. 5 (CITF) and ref. 6 (HPWF) are also shown. The HPWF data differs from ours a) in the kinematic region it covers and b) in the wide neutrino energy spectrum integrated over. The smooth curve is the estimated non-prompt background.

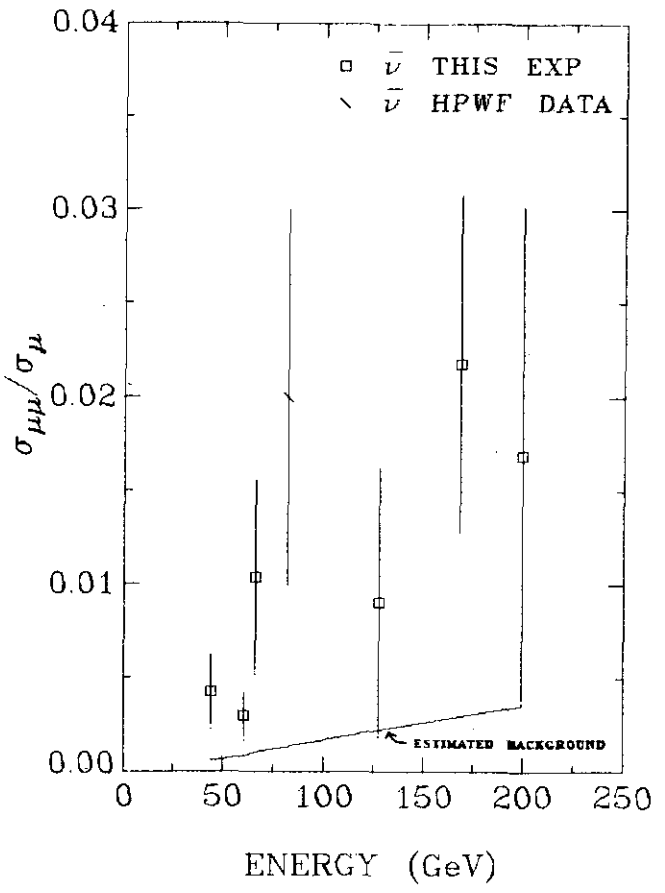

Figure 7 b

The ratio of the dimuon production cross section ($\sigma_{\mu\mu}$) to the single muon production cross section (σ_{μ}) for antineutrino induced events in which the first muon enters the spectrometer and the second muon penetration is greater than 1.8 meters of steel (equivalent to 2.4 GeV) is shown as a function of incident energy. The results described in ref. 6 (HPWF) are also shown. The HPWF data differs from ours a) in the kinematic region it covers and b) in the wide antineutrino energy spectrum integrated over. The smooth curve is the estimated non-prompt background.

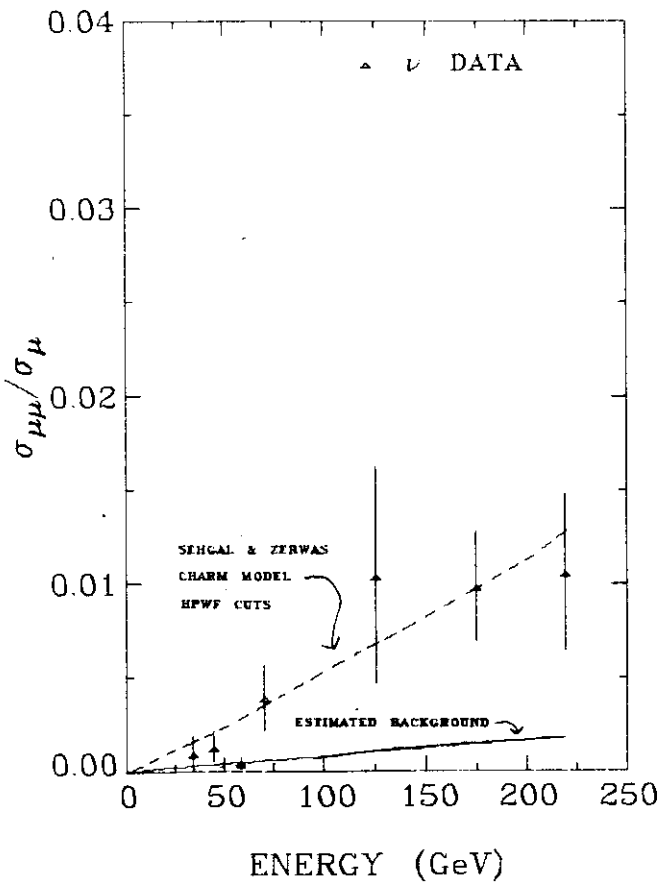

Figure 8 a

The ratio of the dimuon production cross section ($\sigma_{\mu\mu}$) to the single muon production cross section (σ_{μ}) for neutrino induced events in which the first muon enters the spectrometer and the second muon penetration is greater than 2.8 meters of steel (equivalent to 4 GeV) is shown as a function of incident energy. The smooth curve is the estimated non-prompt background. The dashed curve is the result of a charm model calculation[7] with HPWF cuts. It is normalized to the data at 175 GeV.

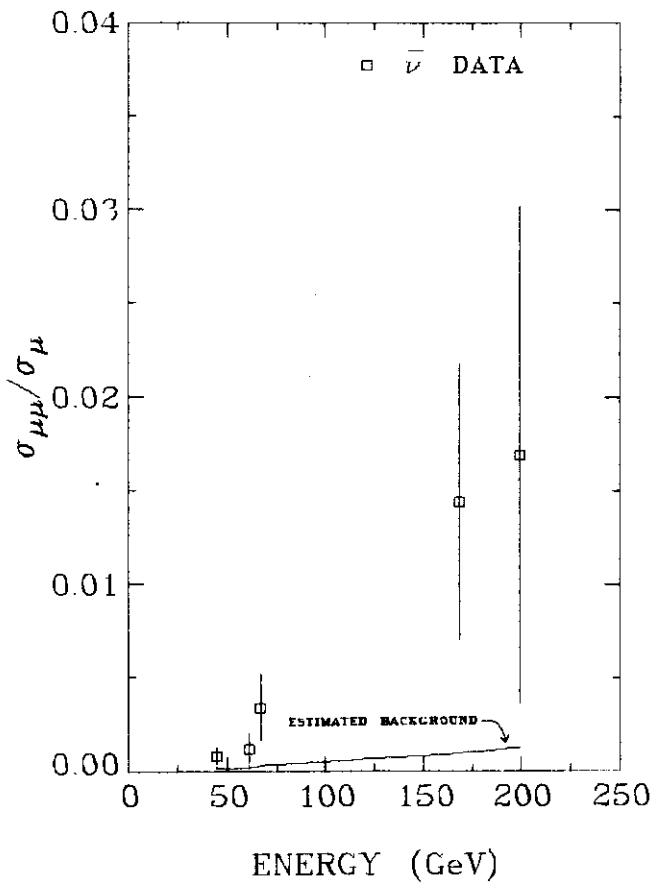

Figure 8 b

The ratio of the dimuon production cross section ($\sigma_{\mu\mu}$) to the single muon production cross section (σ_{μ}) for antineutrino induced events in which the first muon enters the spectrometer and the second muon penetration is greater than 2.8 meters of steel (equivalent to 4 GeV) is shown as a function of incident energy. The smooth curve is the estimated non-prompt background.

the first muon directions. Figure 9 shows the cosine of the angle, $\Delta\phi$, between the two muon momenta projected on the plane perpendicular to the incident neutrino direction. The cosine of this angle is plotted for all events in which the first muon enters the spectrometer and the second muon traverses more than 1.8 meters of steel. $\cos(\Delta\phi)$ would be -1 for events in which the second muon was in the $\mu\nu$ plane. About 50% of the events appear to be correlated with the hadron direction. A similar $\Delta\phi$ distribution has already been seen by HPWF.[6]

VI. Events in Which Both Muons Enter the Spectrometer Magnet

Since the incident beam is sign selected, we can determine if the leading muon charge is the expected charge for a normal charged current event (a "right sign" muon). Figure 10 is a plot of the "right sign" muon momentum versus the "wrong sign" muon momentum for each of the dimuon events in which the muons have opposite charge. The crosshatched areas are regions in which one of the muon momenta is too low to be detected. In approximately 90% of the events, the leading muon has the charge expected for a charged current event.

Figure 11 is a plot of the scaling variables X ($=Q^2/2ME_H$) versus Y ($=E_H/E_\nu$). X and Y are calculated using the total observed dimuon energy for E_ν and the sum of the hadron energy and the second muon energy for E_H. The smooth curves are constant efficiency contours for single muon events at incident energies of 50, 100, and 200 GeV (the solid, dashed, and dotted curves respectively) at $\theta_\mu = 100$ mrad. The detection efficiency is high for events having an X and Y less than the appropriate contour.

The observed average X and Y for the dimuon events are similar to the average X and Y for the single muon events. The average Y is slightly larger and the average X is slightly smaller for the dimuon events relative to the single muon events.

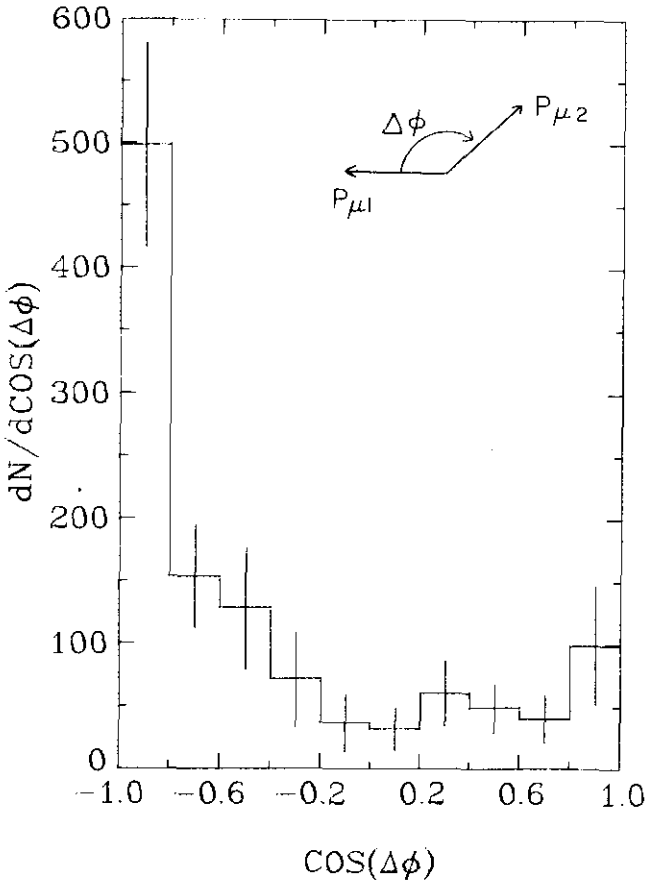

Figure 9

To study a correlation of the second muon direction with respect to the hadron direction, the $\cos(\Delta\phi)$ distribution is shown for those events in which a) the first muon enters the spectrometer and b) the second muon penetrates more than 1.8 meters of steel (equivalent to 2.4 GeV). $\cos(\Delta\phi)$ would be -1 for events in which the second muon was in the $\mu\nu$ plane. About 50% of the events are contained in the peak at $\cos(\Delta\phi) = -1$.

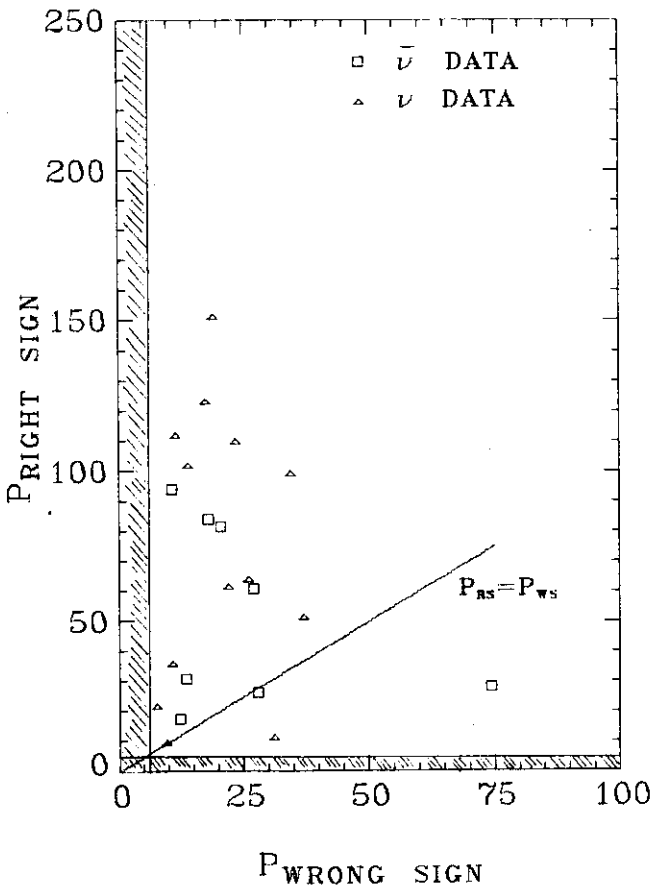

Figure 10

To determine if the leading muon charge is the expected charge for a charged current event (a "right sign" muon), the momentum of the "right sign" muon is plotted versus the momentum of the "wrong sign" muon for those events in which both muons enter the spectrometer and are of opposite charge. In approximately 90% of the events the leading muon has the charge expected for a charged current event.

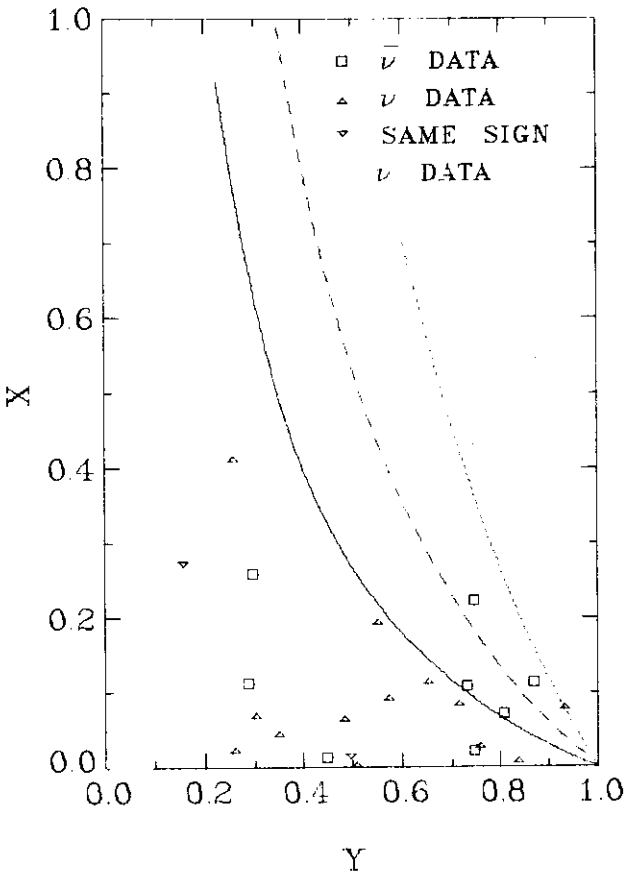

Figure 11

The scaling variable X ($=Q^2/2ME_\nu$) is plotted versus the scaling variable Y ($=E_H/E_\nu$) for those events in which both muons enter the spectrometer. X and Y are calculated using the total observed dimuon energy for E_ν and the sum of the hadron energy and the second muon energy for E_H. The smooth curves are constant efficiency contours for single muon events at incident energies of 50, 100, and 200 GeV (the solid, dashed, and dotted curves respectively) at θ_μ = 100 mrad.

VII. Conclusions Concerning Dimuon Production

In summary, we see dimuon production in both the neutrino and antineutrino data over a wide range of energies. The azimuthally corrected neutrino and antineutrino dimuon production rate relative to the single muon production rate reaches about 1.5% at high energy. The energy dependence of the dimuon signal is consistent with a low mass threshold.

Because of the dichromatic nature of the incident neutrino beam, we can conclude that any energy carried away by unseen leptons is, on the average, less than 15% of the total energy.

The leading muon usually has the charge normally expected for charged current events.

The averages of the scaling variables X and Y are similar to the single muon averages.

VIII. The First Observation of Trimuon Events

Prior to this experiment there has been no reported observation of trimuon production in neutrino or antineutrino data. In this data sample, we have observed two trimuon events. These events were found in the data obtained with the hadron beam energy set to +190 GeV and are shown in figures 12 a,b. Some of the interesting kinematic quantities calculated for these events are indicated in the figures.

Using the event rates at +190 and +250 GeV running, the uncorrected trimuon production rate relative to the single muon production rate is approximately 3×10^{-4}.

The obvious question is whether these events are explained by conventional mechanisms. In the following, we estimate possible sources, using the total number of one muon and two muon events in the +190 and the +250 running.

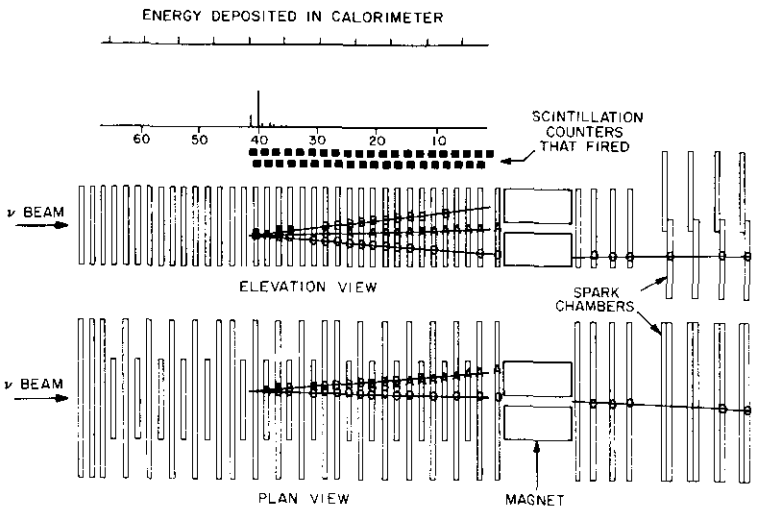

E_{vis} = 90 GeV

E_H = 48 GeV

X = 0.06

Y = 0.66

Q^2 = 5.7 $(GeV/c)^2$

W^2 = 85 $(GeV/c^2)^2$

$E_{\mu o}$ = 30 GeV

$E_{\mu A}$ = 6.1 - 8.6 GeV

$E_{\mu B}$ = 5.3 GeV

M_{oB} = 1.2 GeV/c^2

M_{oB} = 1.7 GeV/c^2

$M_{AB} \geq$ 0.4 GeV/c^2

$M_{oAB} \geq$ 2.2 GeV/c^2

Figure 12 a

A trimuon event observed with a +190 GeV hadron beam. Track 0 traverses the spectrometer magnet and is momentum analyzed. Track A stops in the magnet so that its energy, $E_{\mu A}$, is between 6.1 and 8.6 GeV. Track B stops in the target and, therefore its energy, $E_{\mu B}$, is 5.3 GeV. The observed energy is 90 GeV, hence this event could have come from either a pion-decay (ν_π) or a kaon decay (ν_K) neutrino.

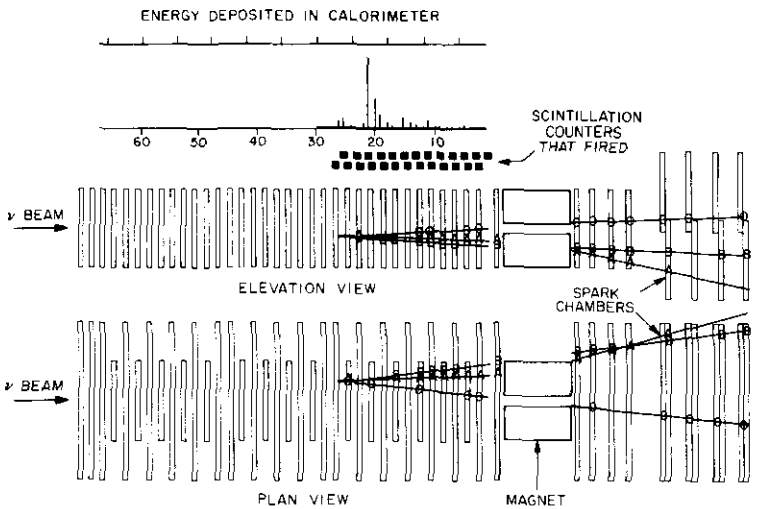

E_{vis}	= 176 GeV	$E_{\mu o}$	= 54 GeV
E_H	= 107 GeV	$E_{\mu A}$	= 10 GeV
X	= 0.22	$E_{\mu B}$	$\geq$ 4.4 GeV/c
Y	= 0.69	M_{oA}	= 2.3 GeV/c^2
Q^2	= 45 $(GeV/c)^2$	M_{oB}	$\geq$ 2.0 GeV/c^2
W^2	= 160 $(GeV/c^2)^2$	M_{AB}	$\geq$ 0.32 GeV/c^2
		M_{oAB}	$\geq$ 3.1 GeV/c^2

Figure 12 b

A trimuon event observed with a +190 GeV hadron beam. Track O and A traverse the magnet and are momentum analyzed. Track B leaves the target, hence $E_{\mu B}$ is a lower limit to its energy. The observed energy is 176 GeV, consequently this event could only have come from a kaon-decay (ν_K) neutrino.

Three possible conventional sources of three-muon events are:

1) Simultaneous pion or kaon decay at the hadronic vertex to produce two extra muons (figure 13a). An upper limit to the expected number of events from this process is ~0.03; this source is considered very unlikely.

2) Neutrino induced dimuon production with a pion or kaon decay at the hadronic vertex to produce an extra muon (figure 13b). An upper limit to the number of events expected from this background is ≤ 0.05 and this explanation is also considered to be very unlikely.

3) "Direct" dimuon production at the hadronic vertex or from nuclear interactions in the hadronic shower (figures 13c and 13d). The uncorrected neutrino trimuon production rate relative to the single muon rate is on the order of 3×10^{-4}. In hadronic collisions the prompt μ/π ratio is $\sim 10^{-4}$. If this prompt signal in hadronic collisions is dimuon production, then this rate is comparable to the observed neutrino induced trimuon signal. This is a possible explanation for the neutrino induced trimuon signal.

IX. Conclusions on Trimuon Production

In summary, two trimuon events were observed and the uncorrected trimuon production rate relative to the single muon production rate is approximately 3×10^{-4}. It is unlikely that the observed trimuon events result from single or double pion or kaon decay in the hadron shower. A possible source is, however, a normal charged current event accompanied by "direct" dimuon production at the hadron vertex or from nuclear interactions in the hadron shower.

a) neutrino induced dimuon production with a π, K decay into a single μ at the hadronic vertex.

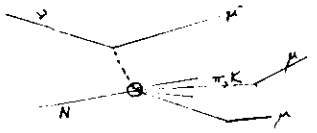

b) two muon production accompanied by π or K decay.

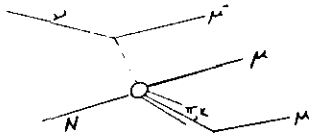

c) prompt dimuon production at the hadronic vertex.

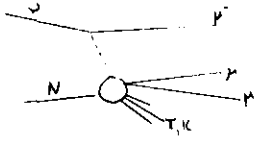

d) prompt dimuon production by fast mesons in the hadronic cascade.

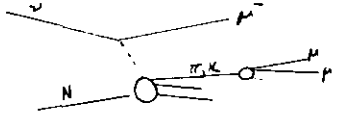

Fig. 13

Possible trimuon sources.

References

1. Talk presented by L. Stutte, CALT 68-564, at the SLAC Topical Conference, Stanford Linear Accelerator Center, Palo Alto, California, Aug. 11-13, 1976.
2. B. C. Barish, CALT 68-835, published in Proceedings of the Sixth Hawaii Topical Conference in Particle Physics, p.213, (1975).
3. B. C. Barish, et al., Fermilab Proposal No. 21, and P. Limon, et al., Nucl. Inst. and Meth. 116, 317 (1974).
4. B. C. Barish, et al., Nucl. Inst. and Meth. 116, 413 (1974) and Nucl. Inst. and Meth. 130, 49 (1975).
5. B. C. Barish, et al., Phys. Rev. Lett. 36, 939 (April, 1976) and A. Bodek, Proceedings of the Summer Institute on Particle Physics, SLAC, (July, 1975).
6. A. Benvenuti, et al., Phys. Rev. Lett. 35, 1199 (Nov., 1975) and Phys. Rev. Lett. 35, 1249 (Nov. 1975).
7. Sehgal and Zerwas, Nucl. Phys. B108, 483 (1976) and Phys. Rev. Lett. 36, 399 (Feb., 1976).